Earthquake Research Advances xxx (xxxx) xxx

Contents lists available at ScienceDirect

Earthquake Research Advances

journal homepage: www.keaipublishing.com/en/journals/earthquake-research-advances

Static-shift suppression and anti-interference signal processing for CSAMT based on Guided Image Filtering

Enhua Jiang [a], Rujun Chen [a,*], Debin Zhu [a], Weiqiang Liu [b], Regean Pitiya [a]

[a] School of Geoscience and Info-physics, Central South University, Changsha, 410083, China
[b] College of Geophysics, China University of Petroleum-Beijing (CUP), Beijing, 102249, China

ARTICLE INFO

Keywords:
CSAMT
Static shift
Guided image filtering
Anti-interference

ABSTRACT

Shallow conductive heterogeneity can lead to static shifts ain the apparent resistivity sounding curve of controlled-source audio-frequency magnetotellurics (CSAMT). The static effect will shift the apparent resistivity curves along with axial log-log coordinates. Such an effect, if not properly processed, can distort the resistivity of rock formation and the depth of interfaces, and even make the geological structures unrecognizable. In this paper, we discuss the reasons and characteristics of the static shift and summarize the previous studies regarding static shift correction. Then, we propose the Guided Image Filtering algorithm to suppress static shifts in CSAMT. In detail, we use the multi-window superposition method to superimpose 1D signals into a 2D matrix image, which is subsequently processed with Guided Image Filtering. In the synthetic model study and field examples, the Guided Image Filtering algorithm has effectively corrected and suppressed static shifts, and finally improved the precision of data interpretation.

1. Introduction

The controlled-source audio magnetotelluric (CSAMT) method is proposed to overcome the disadvantages including the randomness and weak energy of natural field source signals. The method uses a grounded wire or an ungrounded loop as an artificial field source to measure the tangential component of the orthogonal electromagnetic field in the wave region and calculate the Cagniard resistivity (Tang, 2005). CSAMT is widely employed in resource exploration including deep concealed metal mines, groundwater, metal minerals, and oil and gas reservoirs because of its large detection depth and high resolution. However, there is a common and tricky phenomenon called static shift in the actual application of CSAMT (Huang, 2006). To suppress the static shift, we need to conduct a deeper study on the comprehensive improvement of the existing data processing and interpretation methods.

The commonly used filter methods are mainly divided into the following categories: the curve shift method, the spatial filter method, the median filter method, the electromagnetic array profiling (EMAP) method, the phase integration method, the wavelet method, and the joint inversion method. To be specific, Bostick (1986) proposes the magnetotelluric exploration method based on Born approximation (EMAP) to suppress static shifts. Song et al. (1995) introduce the wavelet method to identify and suppress static shifts. Luo (1996) proposes the phase integration method by taking the advantage of the unaffected phase. Yang et al. (2002) point out a static correction method based on impedance tensor, which obtains the electric field distortion tensor and static correction tensor from high-frequency data, and corrects the measured impedance tensor in the full frequency domain. Tournerie et al. (2006) propose a static shift supression approach by using the cooperative Kriging method. Yang et al. (2009) select the directional filter method to suppress static shifts. Yu et al. (2017) propose a static shift correction method based on the combination of the wavelet transform modulus maximum method and the threshold method. Liu et al. (2018) utilize a spatial domain topology processing technique based on field observation data. Luan et al. (2018) successfully conduct the recognition and correction of static shifts based on the Radon transform. Zhamaletdinov

* Corresponding author.
E-mail address: 554035269@qq.com (R. Chen).

Production and Hosting by Elsevier on behalf of KeAi

https://doi.org/10.1016/j.eqrea.2022.100117
Received 23 December 2021; Received in revised form 10 February 2022; Accepted 11 February 2022

Please cite this article as: Jiang, E. et al., Static-shift suppression and anti-interference signal processing for CSAMT based on Guided Image Filtering, Earthquake Research Advances, https://doi.org/10.1016/j.eqrea.2022.100117

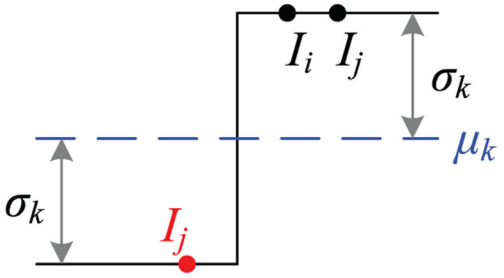

Fig. 1. A 1D example of an ideal step edge (He, 2013).

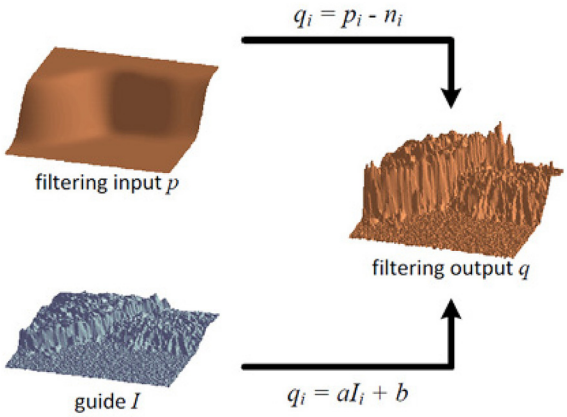

Fig. 2. Schematic diagram of Guided Image Filtering (He, 2013).

(2020) applies a quantitative method in correcting static offset distortion. In this scenario, the static displacement distortion is quantified by comparing the magnetic field with the apparent resistivity curve normalized to the total electric field or total input impedance value. In spite of great progress achieved using the aforementioned methods, their limitations are obvious: Radon transform may causes undercorrection or overcorrection, the wavelet transform may have high calculational cost, and accurate results cannot be acquired rapidly in practice.

In this paper, we propose an algorithm based on Guided Image Filtering (Hereinafter referred to as GIF) to eliminate the static effect in CSAMT data. In practical applications, it has been proved to be more robust and accurate than traditional processing methods. Additionally, it improves the quality of impedance tensor. In addition, theoretical and practical studies have proved that GIF can suppress the static shift effect more effectively compared with other algorithms.

1.1. Static shift

The effect of shallow inhomogeneities on the MT curve is mainly due to the distortion of the electric field caused by the charge accumulated on the surface of the corresponding inhomogeneous bodies. Shallow inhomogeneities can lead to severe problems in the interpretation of magnetotelluric (MT) data by shifting the MT apparent resistivity sounding curve with a scale factor, which is independent of frequency on the standard log-apparent-resistivity versus log-frequency display. The amount of parallel shift is commonly referred to as the MT static shift (Larsen, 1977; Sternberg, 1988; Jones, 1988). If the shifts are not suppressed effectively, large errors may occur in the inverted models of the data, thus producing inevitable errors in geo-electric information or geological structures.

In order to identify and suppress the static shift more efficiently and thoroughly, we summarize the main related features as follows (Cheng, 2008).

(1) On the pseudosection graph, the static effect is shown as vertical intensive ρ isolines, vertical spindle-shaped local closed isolines, or more complex shapes. Overall, it is shown as steep intensive isolines with a small transverse range.
(2) The ρ-f apparent resistivity curve in the axial log-log coordinates is shifted up and down along the ρ axis, but the slope of the apparent resistivity curve and the phase curve of φ-f remains unchanged.
(3) The static shift affects the electric field channel E rather than the magnetic field channel H.
(4) The static effect is independent of frequency.

In addition, the static shift is also manifested in false steep and deep faults or anomaly bodies with large vertical extensions in the qualitative interpretation. The Spatial filter method is one of the most frequently used methods to suppress static shifts and the main concept is that the same transmit frequency signal and the change of Cagniard apparent resistivity along the survey lines caused by the anomaly body should be relatively gentle rather than sharp change associated with static shifts. Therefore, it can be regarded as a local effect caused by a local reason, which can be averaged filtering in the global scope. The method based on the theory of sampling is essential to create a low-pass filter to suppress the static shift by considering it as high-frequency interference. (Huang, 2006). In this paper, we focus on the comparison between the spatial filtering and the Guided Image Filtering in suppressing the static offset.

2. Method

2.1. Guided Image Filtering

Guide Image Filtering adds the detail layer in the guided image I during the filtering process. The final output image Q is similar to the filtering input image P in content, but has a similar outline with the guidance image I. Parameters I and P should be set by the user in advance. When I=P, GIF becomes an edge-preserving filter (He et al., 2010).

In the general linear filtering process, the filtering output at pixel i is expressed as a weighted average:

$$q_i = \sum_{j\in\omega_i} W_{ij}(I)p_j \tag{1}$$

where i and j are pixel indexes, p is the input image pixel, q denotes the output image pixel, the filter kernel W_{ij} is the function of the guidance image I which provides weights for p_j and is independent of p. Kernel weights W_{ij} is explicitly expressed by:

$$W_{ij}(I) = \frac{1}{|\omega|^2}\sum_{k(i,j)\in\omega_k}\left(1+\frac{(I_i-\mu_k)(I_j-\mu_k)}{\sigma_k^2+\varepsilon}\right) \tag{2}$$

where ω_k is a square window with a radius r including pixel i, k is the center position of ω_k, $|\omega|$ is the number of pixels in ω_k, μ_k is the average value of pixels in ω_k, and I_i and I_j are two adjacent pixels value, σ_k^2 represents the variance of pixels in ω_k, and ε is the regularization coefficient.

In Equa. 2, we can obtain the adaptive weight: The terms $(I_i-\mu_k)$ and $(I_j-\mu_k)$ have opposite signs (±) when I_i and I_j are on the different sides of an edge. Thus, the term $1+\frac{(I_i-\mu_k)(I_j-\mu_k)}{\sigma_k^2+\varepsilon}$ is close to zero, and $W_{ij}(I)$ will be reduced; The terms $(I_i-\mu_k)$ and $(I_j-\mu_k)$ have same signs when I_i and I_j are on the same sides of an edge, $W_{ij}(I)$ will be increased (Fig. 1). When two pixels are on different sides of an edge, the weight value will be much smaller than that corresponding the pixels on the same side. The pixels in the non-boundary area will be given a larger weight value, and the filtering effect is obvious. This means the pixels across an edge are almost not averaged together.

The critical point of GIF is based on the local linear relationship between I and P. We consider that a point on a function has a linear rela-

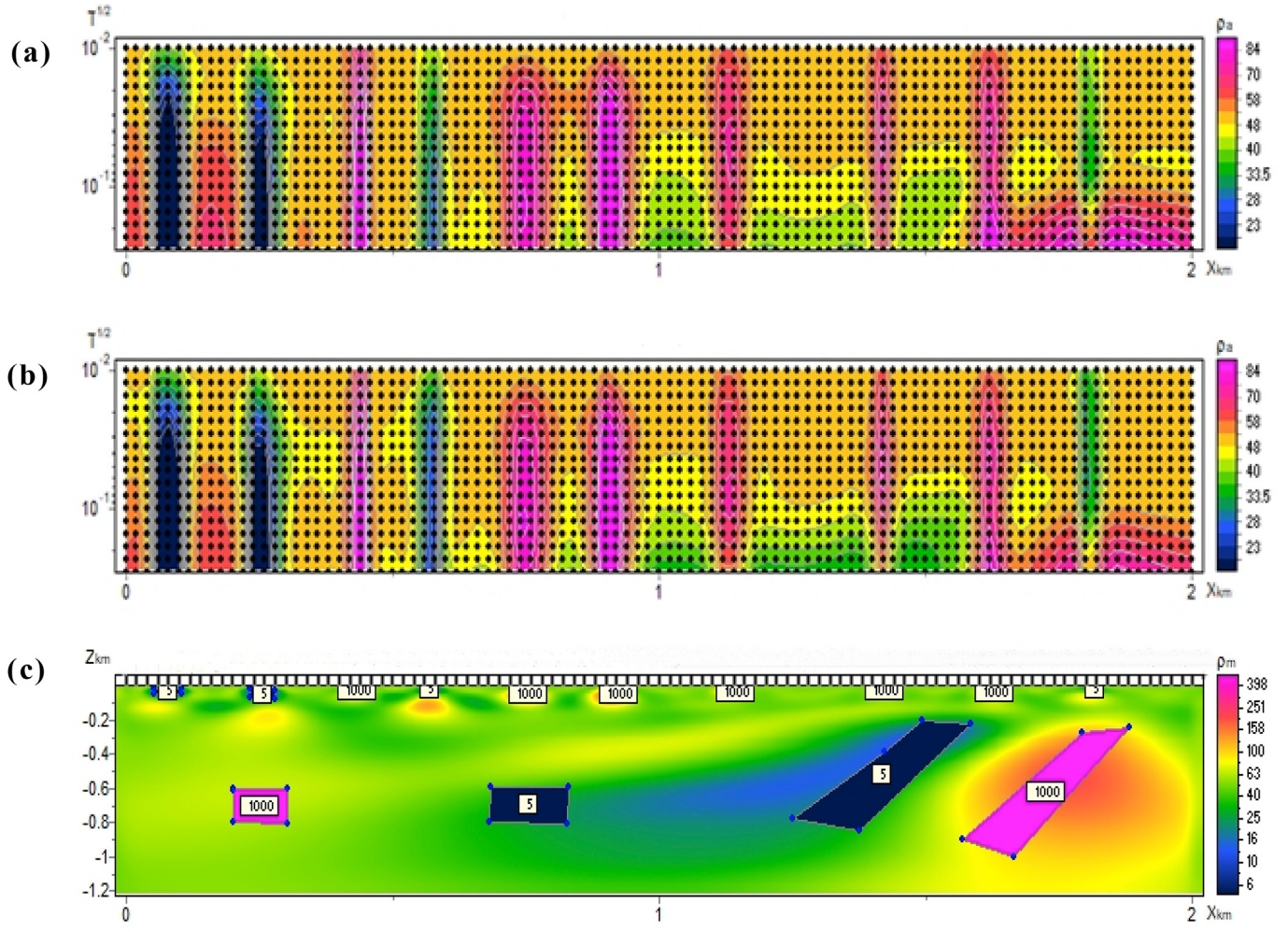

Fig. 3. 2-D CSAMT synthetic survey. (a) Observed apparent resistivity. (b) Calculated apparent resistivity. (c) Polygonal cross-section. Pink polygons: high resistance body model. Blue polygons: low resistance body model. White blocks: CSAMT receivers on the surface.

tionship with its neighboring points, hence a complex function can be indicated using a number of local linear functions. When the value of a point on the complex function is needed, we simply compute the values of all linear functions that contain the point and then average them.

In a similar fasion, an image can be considered as a two-dimensional function that cannot be expressed analytically, and thus a guided filter function that satisfies the linear relationship in a two-dimensional window can be modeled through the following formula:

$$q_i = a_k I_i + b_k, \forall i \in \omega_k, q_i \in Q, I_i \in I \tag{3}$$

where a_k and b_k are the coefficients of the linear function, k is the center point of the window. In Equa. 3, the guidance image I and the output image Q are linear relationships in the window ω_k. Then, we derive Equa. 3 to obtain $\nabla q = a\nabla I$ which proves that q has an edge only if I has an edge in the local linear model. The derivative expression indicates that when the guidance image I contains a local mutation signal (i.e. an edge), the output image Q will be given weight a_k to retain the signal in the corresponding position.

In Fig. 2, to determine the linear coefficients a_k and b_k, constraints from the input p are required. We define the output q as the input p subtracting noise n:

$$q_i = p_i - n_i \tag{4}$$

where n is the noise term, the purpose of linear regression is to minimize n. Combined with Equa. 3, the objective function can be modeled through the following formula:

$$\min_{(a,b)} \sum_{i \in \omega_k} (aI_i + b - p_i)^2 + \varepsilon a^2 \tag{5}$$

In Equa. 5, we search for an optimal value, which is used to minimize the following cost function:

$$E(a_k, b_k) = \sum_{i \in \omega_k} \left((a_k I_i + b_k - p_i)^2 + \varepsilon a_k^2 \right) \tag{6}$$

where ε is the regularization coefficient used to penalize larger a_k values. Equa. 5 is a linear ridge regression model. The coefficients a_k and b_k can be solved by the least square method:

$$a_k = \frac{\frac{1}{|\omega|}\sum_{i \in \omega_k} I_i p_i - \mu_k \overline{p_k}}{\sigma_k^2 + \varepsilon} \tag{7}$$

$$b_k = \overline{p_k} - a_k \mu_k \tag{8}$$

$$\overline{p_k} = \frac{1}{|\omega|} \sum_{i \in \omega_k} p_i \tag{9}$$

where $\overline{p_k}$ is the mean value of the input image P in ω_k.

Since the window has a finite size, the same pixel q_i in the output

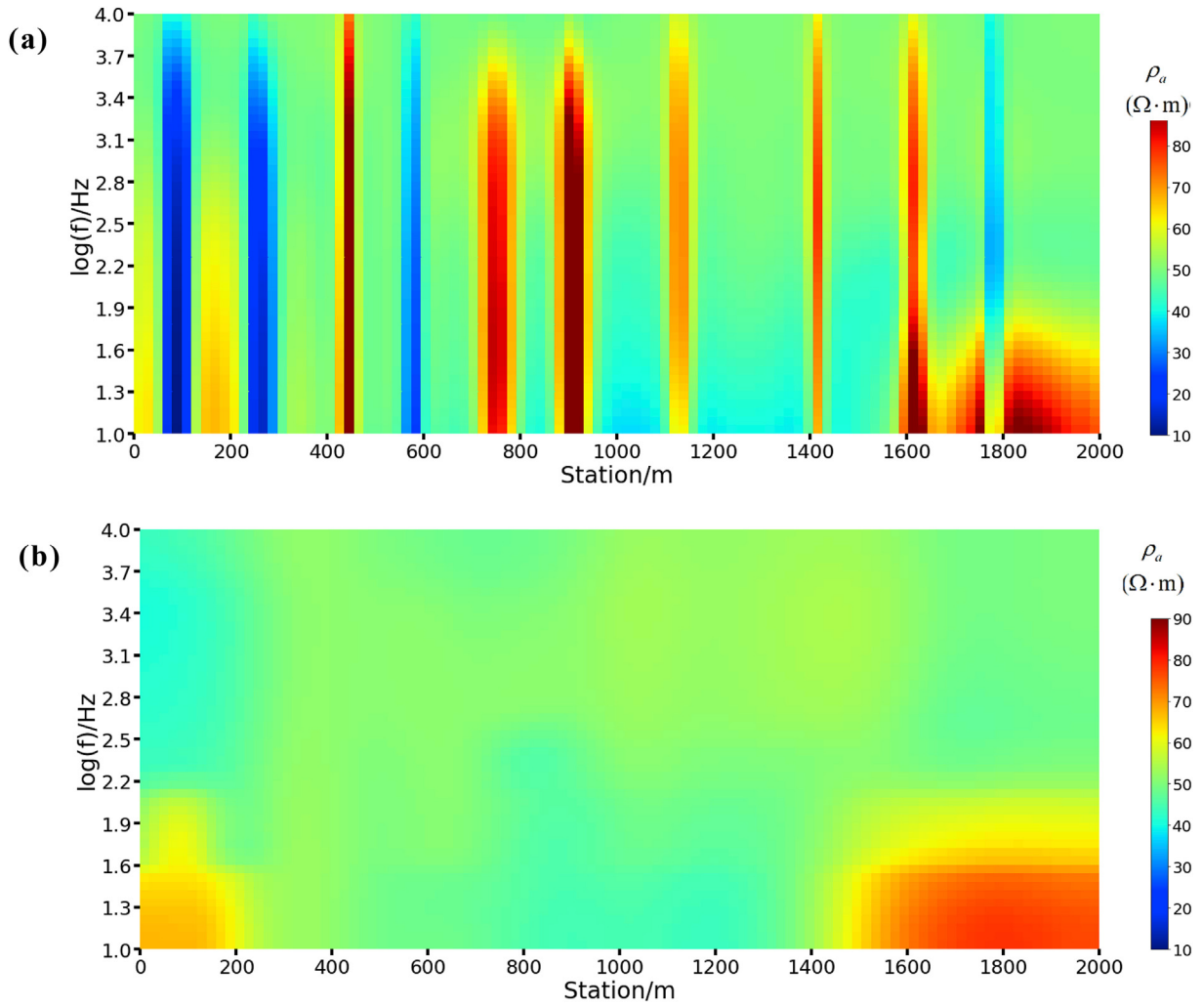

Fig. 4. The Guided Image Filtering method for the suppression of the static shift. (a) Apparent resistivity pseudosection of a 2D model, which is affected by the static shift. (b) The results after Guided Image Filtering.

image Q can be involved in the whole overlapping windows ω_k that covers index i. The values of (a_k, b_k) and q_i are different in other windows. In order to ensure the uniqueness of the result, we average all the values of (a_k, b_k) and q_i, and the final filtering output q_i can be rewritten as:

$$q_i = \frac{1}{|\omega|}\sum_{k|i\in\omega_k}(a_k I_i + b_k) = \overline{a}_i I_i + \overline{b}_i \tag{10}$$

$$\overline{a}_i = \frac{1}{|\omega|}\sum_{k\in\omega_i} a_k, \overline{b}_i = \frac{1}{|\omega|}\sum_{k\in\omega_i} b_k \tag{11}$$

where $\overline{a}_i$ and $\overline{b}_i$ are the average value of a and b in window ω_k.

After averaging, Equa. 10 still satisfies $\nabla q_i \approx \overline{a}_i \nabla I_i$, which means the filtering output q can retain the main edge information in I. Equa. 3 shows that the guided filter output is still the weighted sum of the values in the neighborhood of q_i. The difference is that the value of the weight $W_{ij}(I)$ is independent of P, but a function of I. On the other hand, Equas. 7–9 determine the minimum error between Q and P, and therefore Q retains the characteristics of both I and P (Dai, 2018).

Equas. 6–11 indicate that the guided filtering effect is determined by two parameters: window radius *rad* and regularization coefficient ε. The larger the *rad* is, the more obvious the filtering effect is, and vice versa. The regularization coefficient ε determines the range of the linear coefficients a_k and b_k and makes the results robust. The larger the ε is, the better the edge-preserving effect is, when *rad* remains constant.

A main advantage of the guided filter is that it naturally has an $O(n)$ (in the number of pixels N) time nonapproximate algorithm, independent of the window radius r and the intensity range ε (He et al., 2013).

2.2. Multi-window overlay

In this paper, we use the multi-window overlay to convert the estimated impedance into a 2D matrix image. The principle of a Multi-window overlay is to suppress interference by extending the observation time and increasing the number of overlays. The main concept is that when processing the CSAMT signals, the apparent resistivity is obtained by selectively averaging a series of individual estimates of the fixed spectral window length of the previous periods. This method has experienced another level of robust weighted average estimation which can identify and remove poor-quality data, and choose high-quality data for subsequent processing, thereby greatly reducing calculation errors and improving calculation accuracy (Liu, 2016). Adding the multi-window superposition method to the robust estimation can effectively suppress unstable interference such as strong interference noise.

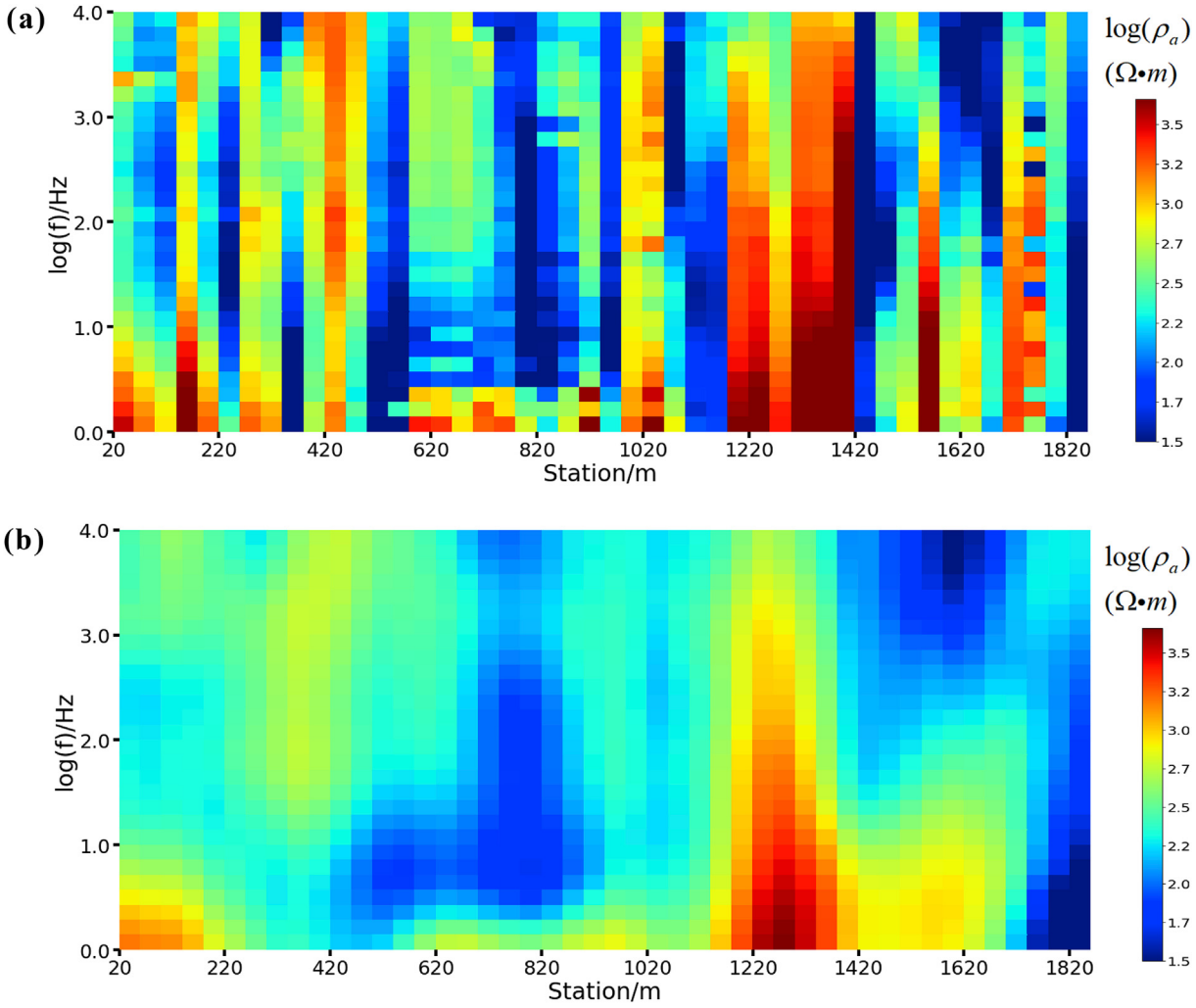

Fig. 5. A practical example of CSAMT apparent resistivity. (a) Original CSAMT apparent resistivity. (b) CSAMT apparent resistivity after GIF. (c) Original CSAMT phase. (d) CSAMT phase after GIF.

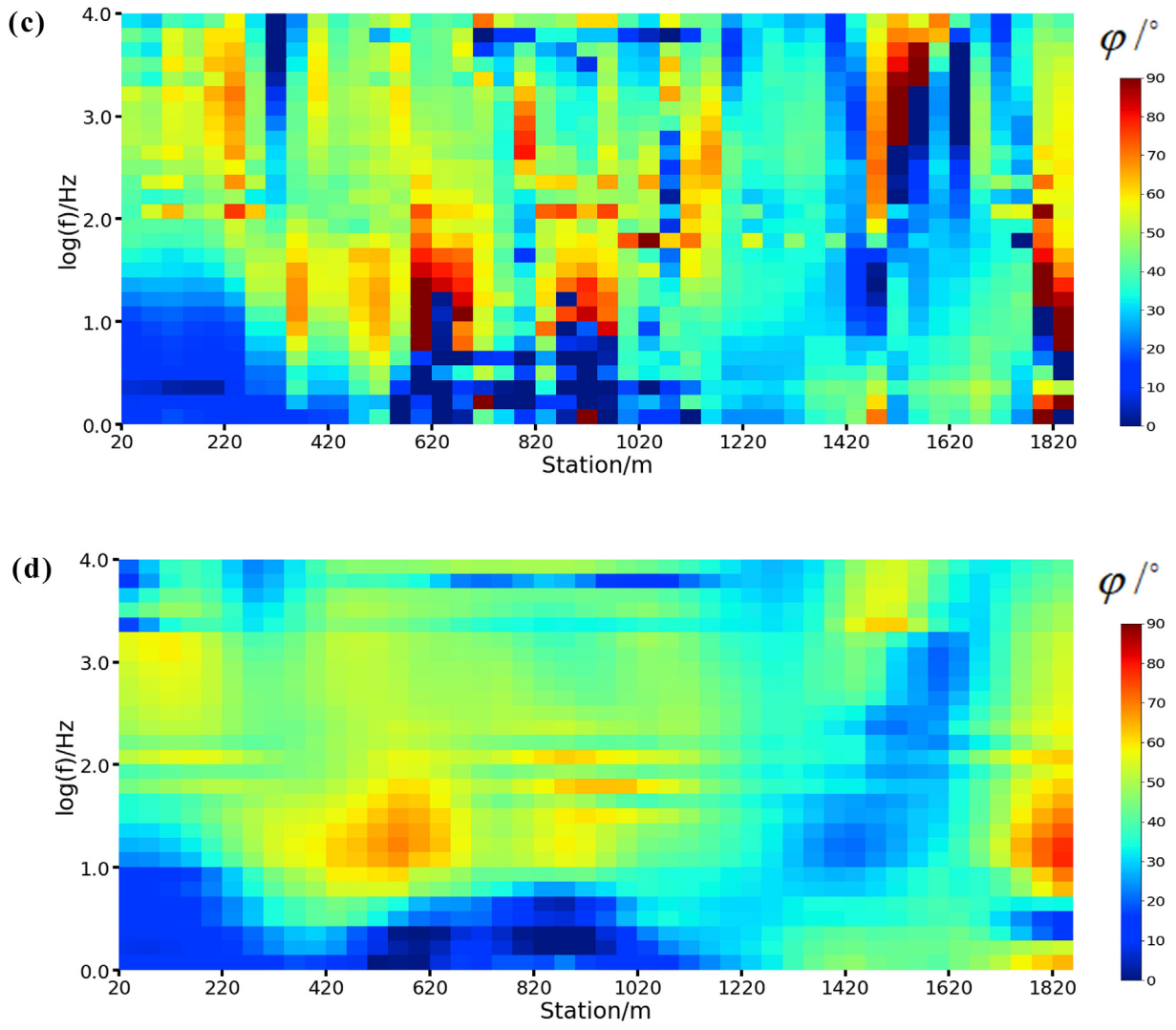

Fig. 5. (*continued*).

3. Results

3.1. Synthetic model study

In this section, we demonstrate the Guided Image Filtering method for static shift removal using a synthetic model. Fig. 3 represents ten small bodies (near the surface), which can cause the static shift, with the resistivity 5 Ω · m (low resistance), the size 100 × 20 m^2 or 1 000 Ω· m (high resistance), the size 100 × 40 m^2 and the site of X = 100, 280, 440, 600, 760, 940, 1 160, 1 440, 1 640 and 1 840 m, respectively.

The resistivity of the background is 50 Ω · m, while the resistivity of anomalous bodies is 5 Ω · m and 1000 Ω · m with a depth of 700 m, with a rectangle size of 200 × 120 m^2 and a quadrilateral size of 140 × 600 m^2 under the site. A 2000-m-long survey line with a 20-m spacing from 0 to 2000 m is deployed on the surface. The transmit frequency distributes from 10^1 to 10^4 Hz in logarithmic space.

Regarding the apparent resistivity pseudosection obtained by 2D forward modeling, the static shift caused by two high-resistivity bodies and two low-resistivity bodies are prominent at the site of X = 0–200, 1 000–1 500, 1 600–2 000 m, as shown in Fig. 3(a). Ten adjacent vertical lines can be observed on the apparent resistivity pseudosection, severely cutting the response of the low-resistivity anomaly body into eleven parts. If these ten lines are not removed, they may be misunderstood as ten vertical anomaly bodies, thus veiling the original deep anomaly body.

Guided Image Filtering is conducted on the apparent resistivity pseudosection according to (3), while the values of the parameters r and ε are determined by (6). In this paper, we select the best result with $r = 6$ and $\varepsilon = 0.5^2$ by repeating numerous times of experiments. Fig. 4(b) shows that the ten lines in Fig. 4(a) have been completely removed, validating the effectiveness of our Guided Image Filtering algorithm. After processing, the static shift is successfully suppressed and the anomaly signals are attributed to the real situation corresponding to the modeling.

3.2. Field examples

In this section, GIF is applied to practical CSAMT data. We select a multi-window overlay to transform data from 1D to 2D. There are a total of 28 frequencies and 46 stations, and thus the format is a 2D matrix. Fig. 5 (a) and Fig. 5 (c) are the original apparent resistivity and phase, Fig. 5 (b) and Fig. 5 (d) are the apparent resistivity and phase after GIF with $r = 6$ and $\varepsilon = 0.5^2$.

By comparing the results before and after filtering, it is obvious that there is no vertical line through all frequencies in Fig. 5, and the outline of the anomalous bodies is observed. The calculated impedance differences between different frequencies and windows become extremely small. Meanwhile, the high-frequency noise is also suppressed greatly,

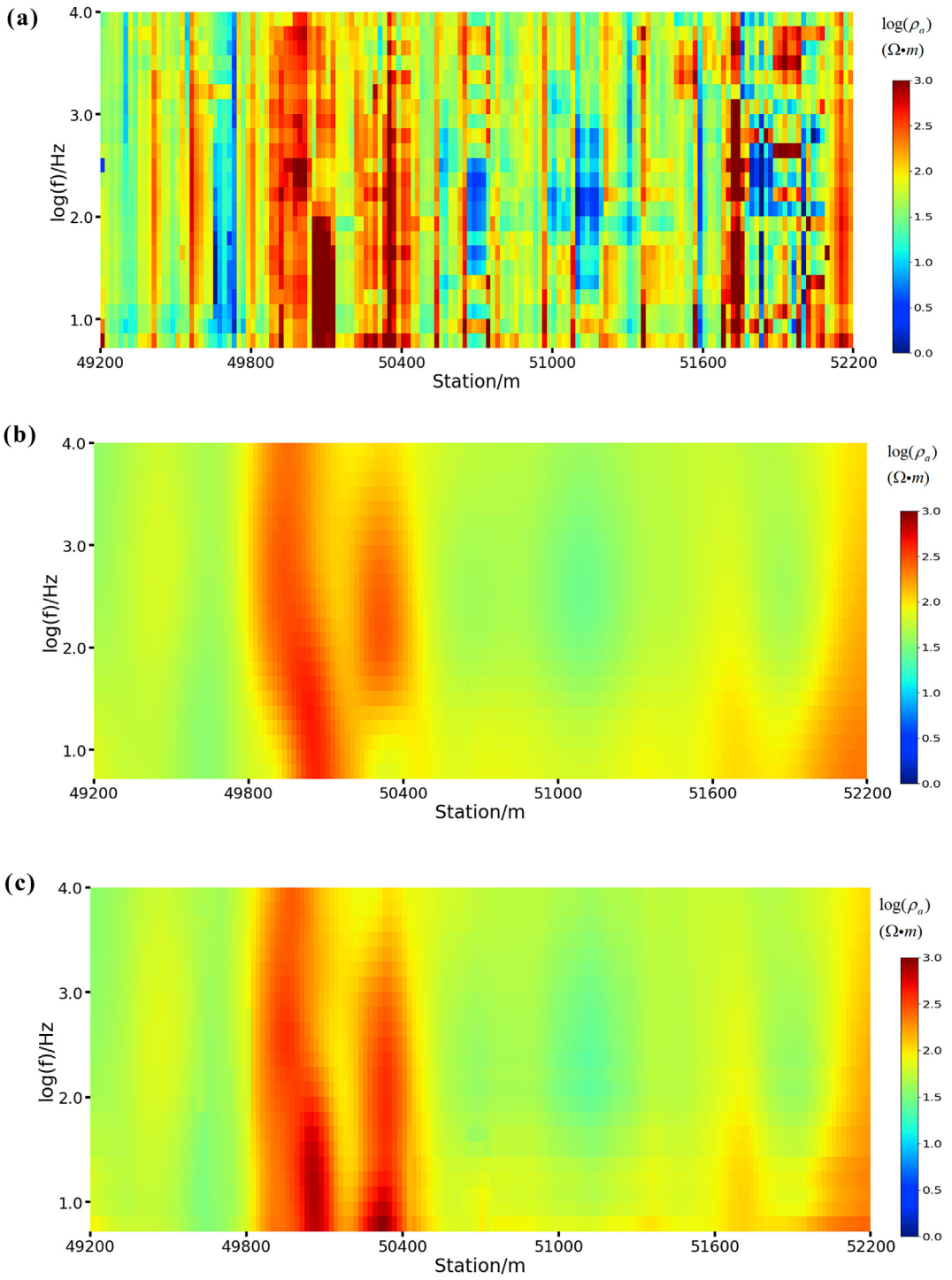

Fig. 6. Comparison of Guided Image Filtering and Radon transformation. (a) CSAMT apparent resistivity from the Weibaoshan tunnel (Luan, 2018). (b) The corrected result using the Radon transformation. (Luan, 2018). (c) The corrected result using the Guided Image Filtering.

generating more smooth, uniform, and continuous 2D images, together with well-preserved edge information while filtering. The results prove that the GIF can be successfully applied into the field of magnetotelluric signal processing.

3.3. Comparison with the Radon transformation method

Fig. 6(a) shows the original apparent resistivity from the Weibaoshan tunnel. Fig. 6(b) and (c) show that the Radon transform method is highly violent. While removing the static effect, it also filters out the edges of the anomaly body, ignoring the protection of the contour edges of the anomaly bodies and resulting in distortion of the filtering results. However, the Guided Image Filter algorithm we proposed takes this into account. GIF can well retain the edge information of anomaly bodies as well as achieving a static shift suppression effect similar to the Radon transform method.

3.4. Comparison results with different parameters

Fig. 7 indicates why the window radius r is more decisive than the

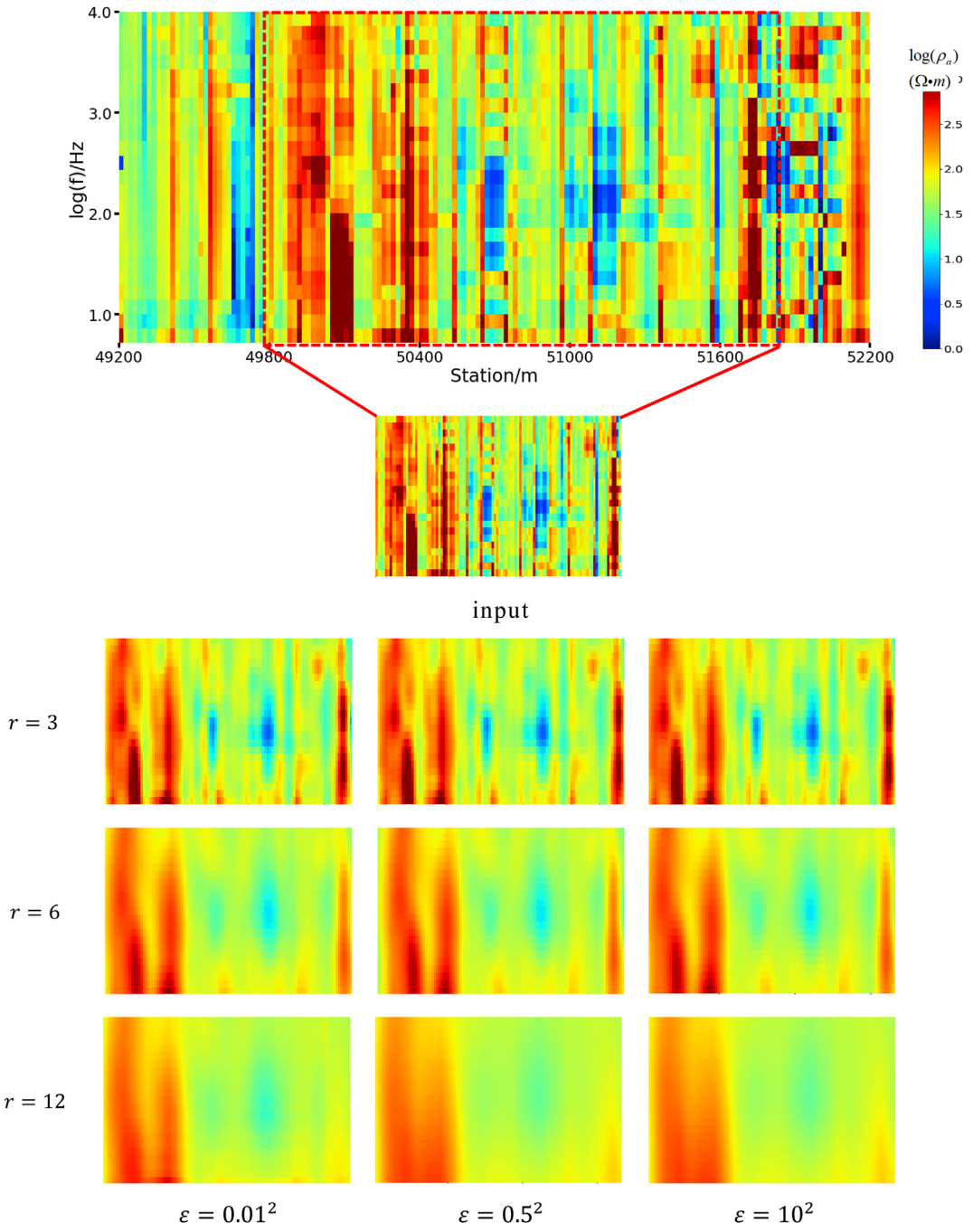

Fig. 7. GIF with different r and ε parameters.

regularization coefficient ε: due to the much smaller data size compared with the size of the image pixel data in the digital image field, the regularization coefficient ε embodied in the more subtle edge changes under the premise of large data size, which can reach the millimeter level in the digital image field. The window radius r is a parameter that determines the local filtering scale which applies to data of any scale and can achieve a relatively obvious filtering effect. The principle of parameter selection is detailed in He (2013).

In the following research, we focus on the influence of the selection of window radius r on the filtering effect. We perform an experiment to study the quality of three strategies: (a) $r = 3$(undersaturation with smaller r); (b) $r = 6$(not bad choice); (c) $r = 12$(oversaturation with larger r).

As shown in Fig. 8, with the increase of window radius r, the filter degree increases, and the image becomes smoother. In the extreme case of small r, the static shift and the random interference are not completely filtered out. In the extreme case of large r, static shift and random interference are completely suppressed, but the filtering results are largely distorted and the effective information of the anomaly bodies is destroyed. The optimal r value is obtained by minimizing the cost function $E(a_k, b_k)$ and solving the linear ridge regression model. In this case, the filtering result not only preserves the effective information of the anomaly body edge, but also thoroughly suppress the static shift and the random interference. Finally, we obtain the best filtering effect.

3.5. Suppressing effect of CSAMT static shift

Numerous scholars have proposed a variety of static shift correction

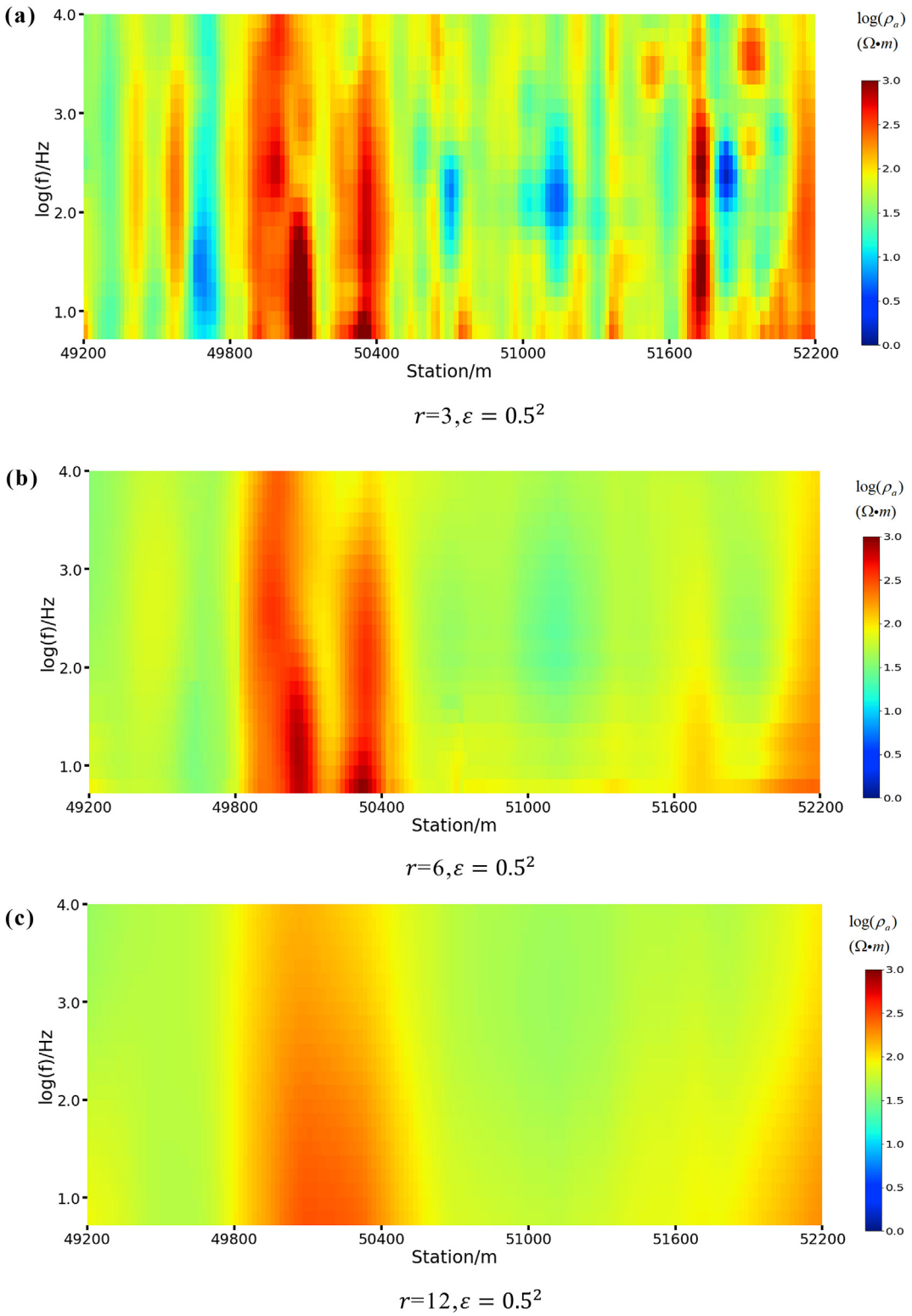

Fig. 8. GIF effect with different parameters. (a) $r = 3$, $\varepsilon = 0.5^2$,(b) $r = 6$, $\varepsilon = 0.5^2$,(c) $r = 12$, $\varepsilon = 0.5^2$

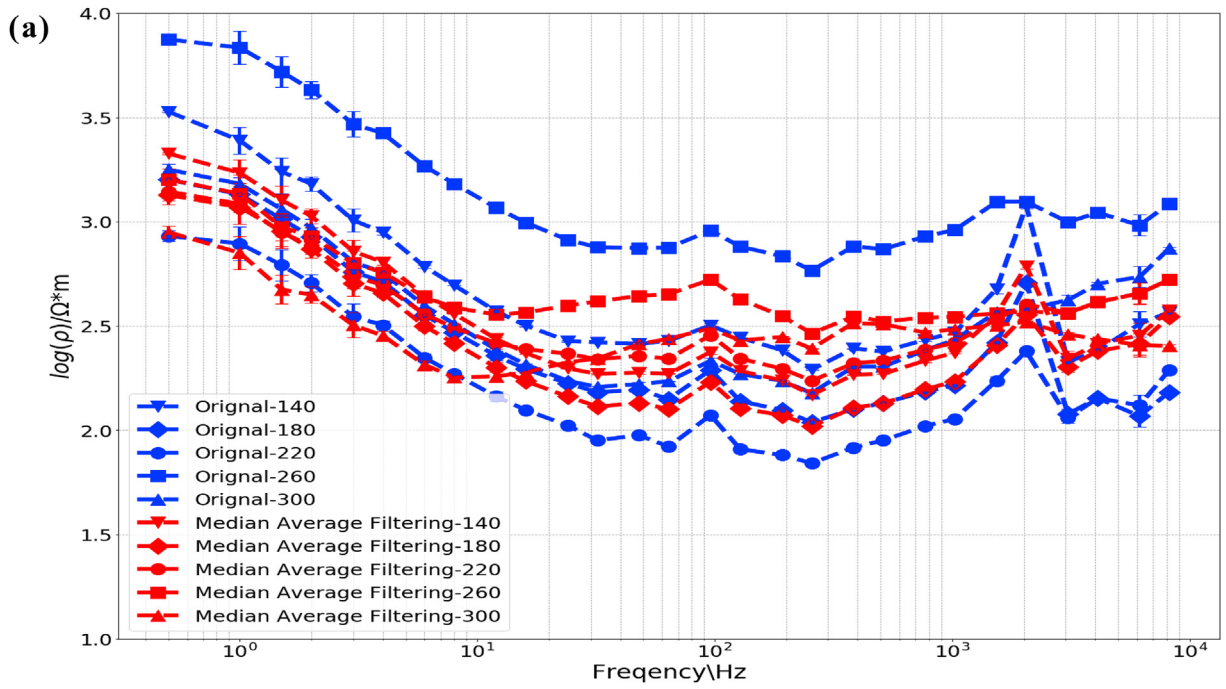

Fig. 9. Comparison of results of GIF and the spatial filtering method to suppress static shifts. (a) CSAMT apparent resistivity after the five-point median average filtering method (5 sites). (b) CSAMT apparent resistivity after the five-point spatial filtering method (5 sites). (c) CSAMT apparent resistivity after GIF (5 sites).

methods. We can classify these relatively important methods into three categories: (1) Static correction using magnetic field component measurement results; (2) Static correction using phase measurement results. (3) Static correction using digital filtering in the spatial or wavenumber domain (Luo et al., 1991).

The spatial filtering method is a low-pass filtering method based on the spatial average. The key of correction depends on the selection of window width and filtering coefficient. By using the spatial filtering method, we can choose different parameters to calculate different results for analyses and comparisons. As long as we select a good filter window coefficient, the static shift can be suppressed effectively. From the principle of removing static shifts, GIF belongs to the category of spatial filtering method, and thus we will compare GIF with spatial filtering methods in this paper.

Given that the static shift is obvious at the CSAMT sites 220, 500, 540, 940, 1 060, and 1 540 (Fig. 3), we select site 220 as an example for specific analysis and combine the adjacent CSAMT sites 140, 180, 260, and 300 for static shift correction. Fig. 9(a) is the apparent resistivity curve after 5-point median filtering. Fig. 9(b) is the apparent resistivity curve after 5-point spatial filtering. Fig. 9(c) is the apparent resistivity curve after GIF. In terms of parameter selection, five-point filter window width D = 5, the digital filter coefficient value $F_k = 0.12, 0.22, 0.32, 0.22,$ and 0.12, respectively. GIF uses original data (un-processed resistivity and phase data) as guidance data, with a window radius $r = 6$ and a regularization coefficient $\varepsilon = 0.5^2$.

Fig. 9(a) shows that the $\rho - f$ apparent resistivity curves are shifted up and down along the logarithmic ρ axis, and the slope of the apparent resistivity curve remains unchanged. This phenomenon is consistent with the characteristics of the static shift.

In Fig. 9(a)-9(c). We can intuitively observe the suppression effect of three different algorithms on the static effect of the 220 sites. The median filtering method absolutely removes high-frequency random noise and has a good suppression on the static effect in the high-frequency band. However, the overall curve fitting is worse than that of other methods; the five-point spatial filtering method performs better static effect correction level than median filtering in the mid-frequency band (10^2 Hz), but is not as good as the results obtained by the median filtering method in the high-frequency band. The proposed Guided Image Filtering algorithm has achieved the best results. The degree of curve fitting is the highest, and the five curves are approximately fitted into a single one. The resolution in the mid-range (10^2 Hz) region is higher than that of the previous methods. GIF shows the most superior static effect correction performance in the whole frequency bands.

Through the analysis of practical CSAMT data, GIF can indeed effectively suppress the common static effect in CSAMT. In addition, the accuracy of the inversion determine the production results in actual exploration. Therefore, it is of great significance to determine the boundary of the underground anomaly body. The edge-preserving feature of GIF can ensure that a good static effect correction result is obtained without destroying the integrity of the boundary of the anomaly body while retaining the information of the anomaly as much as possible.

4. Conclusion

In this paper, we propose a novel method named Guided Image Filtering to suppress static shifts and interference effects in CSAMT. The principle and idea of this method are highly consistent with the spatial filtering method. The key to the filtering effect is the parameter selection of the window radius r and the regularization coefficient ε. Through the analyses of synthetic models and real data, we find that the Guided Image Filtering algorithm can effectively suppress the static shift.

Based on the principle of multi-window overlay, 1-D data are periodically superimposed into a 2-D matrix image. Then, we apply the Guided Image Filtering algorithm to effectively suppresses the static shift in CSAMT. Meanwhile, the edge-preserving feature of Guided Image Filtering can ensure that a good static effect correction result is obtained without destroying the integrity of the boundary of the anomaly body, while retaining the information of the anomaly as much as possible. Both the resistivity and the phase curves show excellent static effect correction performance, further validating our conclusion.

The proposed method improves the data quality and proves the feasibility and superiority of the Guided Image Filtering algorithm in

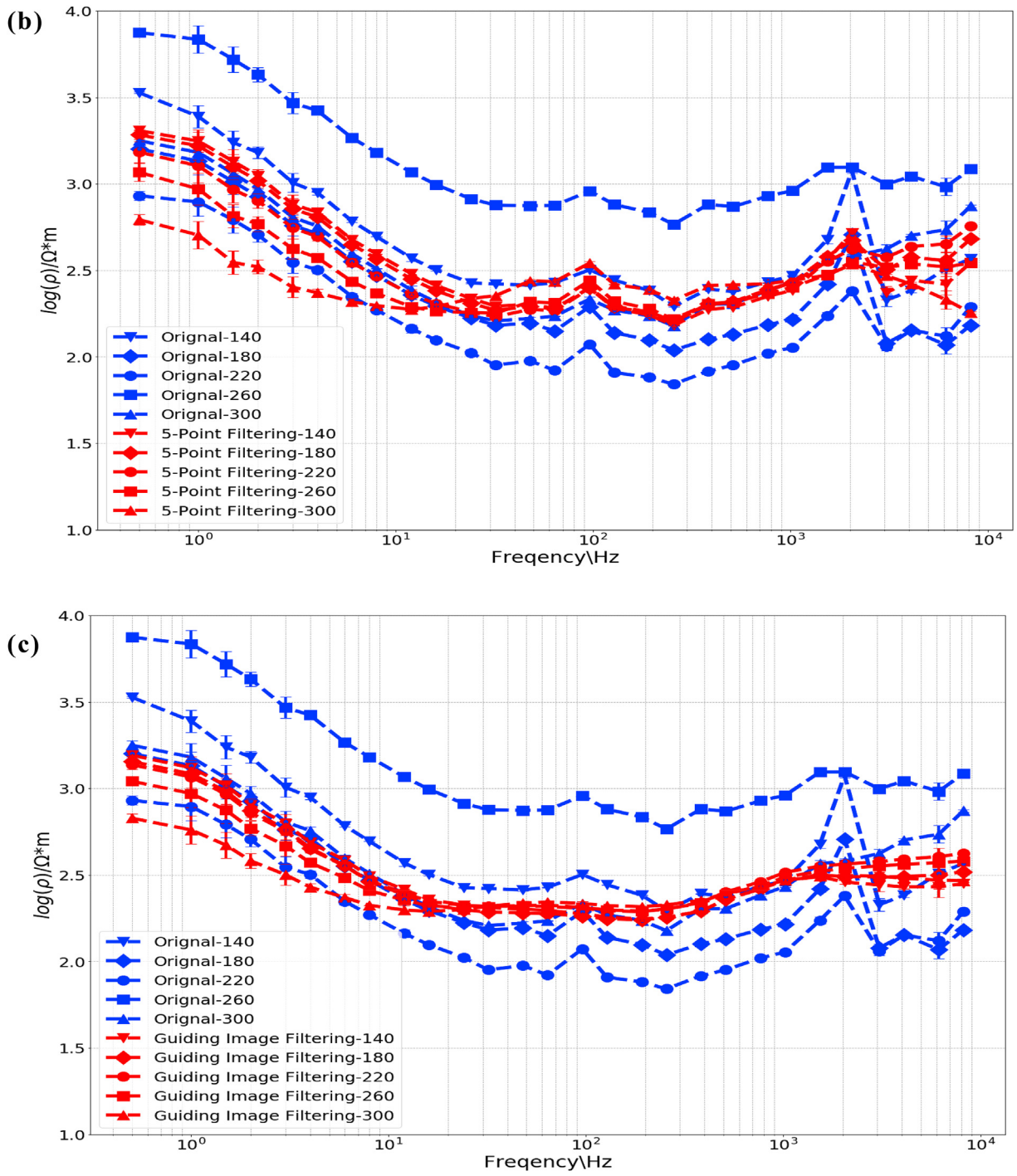

Fig. 9. (*continued*).

anti-interference signal processing. Essentially, the method is based on the statistical characteristics of data. Big data will lead to more accurate results. This method is often applied to the 1D or 2D case. In theory, it can be applied to the 3D case by expanding the dimensionality of the mathematical formulation, which is a good goal for future research. In addition to suppressing static shifts, theoretically, Guided Image Filtering can also be applied to the data processing field of other geophysical methods due to its innovativeness and practicality.

Conflict of interest

The authors declare that there is no conflict of interests regarding the publication of this article.

References

Bostick, J.F., 1986. Electromagnetic array profiling (EMAP)[M]//SEG technical program expanded abstracts 1986. Soc. Explor. Geophys. 60–61.

Cheng, Y., 2008. Identification and Correction of Static Effects of CSAMT. Central South University.

Dai, Q., 2018. Application Research of Edge-Preserving Image filtering[D]. Wuhan University.

He, K., Sun, J., Tang, X., 2010. Guided image filtering. In: European Conference on Computer Vision. Springer, Berlin, Heidelberg.

He, K., Sun, J., Tang, X., 2013. Guided image filtering[J]. IEEE Trans. Pattern Anal. Mach. Intell. 35 (6), 1397–1409.

Huang, Z., 2006. Research on Static Problems and Related Inversion in CSAMT method [D]. China University of Geosciences, Beijing.
Jones, A.G., 1988. Static-shift of magnetotelluric data and its removal in a sedimentary basin environment. Geophysics 53, 967–978.
Larsen, J.c., 1977. Removal of local surface conductivity effects from low frequency mantle response curves. Acta Geod. Geophys. Montanistica Acad. Sci. Hung. 12, 183–186.
Liu, W., Chen, R., 2016. Coherence analysis for multi-frequency IP signal processing under strong interference background[J]. Chin. J. Nonferrous Metals (3), 655–665.
Liu, G., Ma, W., Liu, J., et al., 2018. Research on spatial domain topology processing technology of magnetotelluric sounding static shifts[J]. Geophys. Geochem. Explor.
Luan, X., Di, Q., Cai, H., et al., 2018. CSAMT static shift recognition and correction using radon transformation[J]. Geosci. Rem. Sens. Lett. IEEE 15 (7), 1001–1005.
Luo, Y., He, Z., Ma, R., et al., 1991. Static shift correction of controllable source audio frequency magnetotelluric method[J]. Geophys. Geochem. Explor. 15 (3), 196–202.
Song, S., Tang, J., He, J., 1995. Identification, separation and suppression of static shift in wavelet analysis and electromagnetic sounding [J], 001 Chin. J. Geophys. 120, 000.
Sternberg, B.K., Washburne, J.C., Pellerin, L., 1988. Correction for the static shift in magnetotellurics using transient electromagnetic soundings[J]. Geophysics 53 (11), 1459–1468.
Tang, J., He, J., 2005. Controllable Source Audio Magnetotelluric Method and its Application [M]. Central South University Press.
Tournerie, B., Chouteau, M., Marcotte, D., 2007. Magnetotelluric static shift: estimation and removal using the cokriging method[J]. Geophysics 72 (1), F25–F34.
Yang, S., Bao, G., Li, A., 2002. Static shift and impedance tensor static correction method in MT method[J]. J. Cent. S. Univ. Technol. 33 (1), 8–13.
Yang, N., Wang, Z., Yang, J., 2009. Static correction of CSAMT data with directional filtering method[J]. Comput. Tech. Geophys. Geochem. Explor. 31 (2), 113–116.
Yu, S., Zheng, J., Gao, M., et al., 2017. CSAMT static correction based on wavelet transform modulus maximum method and threshold method[J]. Chin. J. Geophys. 60 (1), 360–368.
Zhamaletdinov, A.A., 2020. A method for quantifying static shift distortions using a magnetic field of controlled source (CSAMT)[J]. Seism. Instrum. 56 (5), 555–563.